Energy Proceedings
Vol 29, 2022
ISSN 2004-2965

Effect of Cathode Composition and Pt-Loading on the Performance of PEMFCs[#]

Asal Saeidfar[1], Serhat Yesilyurt [1*]

[1]*Sabanci University, Faculty of Engineering & Natural Sciences, Istanbul, Turkey*

ABSTRACT

A two-dimensional, multiphase, non-isothermal model is utilized for the design of cathode catalyst layer polymer electrolyte membrane fuel cell (PEMFC) model coupled with a developed homogenous model which considers the catalyst layer (CCL) design parameters. The model is applied to predict the polarization curves for a variety of cathode compositions. It is found that increasing the radius of CCL influential particles including Pt and carbon particles, deteriorates the performance while increasing the ionomer weight percentage in CL enhances the performance of the cell.

Keywords: PEMFC, modeling, performance analysis, cathode catalyst layer, microstructure, low platinum loading

1. INTRODUCTION

Polymer electrolyte membrane fuel cells (PEMFCs) are envisioned as the ultimate power sources of future vehicles owing to several merits including the high power and energy density, zero-emission, quick response time [1]. Due to extensive theoretical and experimental research, some of the remarkable challenges to the commercialization of PEMFCs have already been addressed. However, the large-scale deployment of PEMFCs is pertinent to curtailing the loading of platinum (Pt) group materials in the catalyst layer (CL) to overcome the cost issues.

Vast R&D efforts have focused on the reduction of Pt loading and the development of alternative electrocatalysts matching high oxygen reduction reaction (ORR) activity and increasing the Pt utilization through novel material design [2]. At low Pt loadings, the CL transport resistance is reported to increase due to the reduction of active sites, as well as the increased flux near each active site [3]. Mathematical modeling and numerical simulation are useful in assessing the transport resistances and optimizing the CL structure to include both micro/macro scale transport processes. The agglomerate model is one of the commonly used methods assuming the aggregation of Pt particles on the surface of primary carbon particles, in which the whole is wrapped with a larger ionomer film [4]. Recently, Hao *et al.* [5] developed a CL model that accounts for interfacial resistances of Pt particles and ionomer film as well as the diffusion resistance of oxygen in the ionomer. However, authors assumed that the produced water is in vapor form. While some researchers attributed the source of increased transport resistance to the thin-film properties of the ionomer, such as water uptake [6], ionic conductivity [7], and oxygen permeability [8], others mentioned higher flooding levels in CL and gas diffusion layer (GDL) owing to reduced vaporization capability [9]. The transport resistances are not only dependent on the Pt loading but also on the cathode structural characteristics. In this regard, Owejan *et al.* [10] reported notable performance losses by diluting Pt catalysts with bare carbon particles.

In addition to CL design parameters, the phase change process, and the transport of water in liquid or vapor form through porous layers are of great importance. The commonly used models for liquid water transport either use Leverett J-function to relate saturation and capillary pressure with Darcy's law or use the microstructural based closure equations such as pore size distribution (PSD) [11,12]. In this regard, Weber *et al.* [12] developed a PSD model using identical hydrophilic (HI) and hydrophobic (HO) pore distributions assuming that the pores are bundles of rejoined cylindrical capillaries. Later, Villanueva [13] used distinct PSDs and discrete contact angles for HI and HO pores, and the effects of microstructural parameters of CL and GDL are studied through a mathematical model [11].

For engineering and design purposes, the computational efficiency of the model and its ability to reproduce experimental findings are equally noteworthy. Rizvandi *et al.* [14] developed a pseudo-three-dimensional (P3D) model using the resistive relationships for the through-plane direction while the fuel cell plane has been assumed to be a thin 2D layer. In this study, the improved cathode electrochemical kinetics model mainly based on [5], as well as the mixed wettability PSD two-phase model, are incorporated into the P3D non-isothermal model accounting for the coupled transport pro-

cesses and the influential cathode microstructural parameters. The effect of CL design characteristics including carbon (C) support radius, I/C ratios, Pt particle radius, and mass fraction of bare carbon is further investigated.

2. MATERIAL AND METHODS

2.1 Computational Domain

A two-dimensional computational domain including the straight channels, GDLs, CLs, and ribs is considered. The computation domain is assumed to be projected on a single surface as shown in Fig. 1. Due to the symmetry, the channels and ribs of the cathode and anode sides overlap.

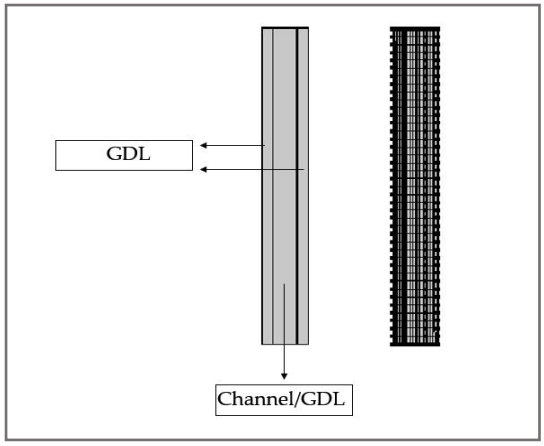

Fig. 1 Schematic of the computational domain and the mesh

The related physical/geometrical parameters utilized in this study are reported in Table 1.

Table 1

Geometric and physical parameters

Description	Parameter	Value
Channel length, width, height [10]	$\mathrm{L_{ch}}, \mathrm{w_{ch}}, \mathrm{h_{ch}}$	10, 0.5, 0.7 mm
Land width [10]	$\mathrm{w_{rib}}$	0.5 mm
Thicknesses of GDL, CL, MEM [5]	$\delta_{\mathrm{GDL}}, \delta_{\mathrm{CL}}, \delta_{\mathrm{m}}$	160, 11, 18 μm
Porosities of GDL, CL [15]	$\varepsilon_{\mathrm{GDL}}, \varepsilon_{\mathrm{CL}}$	0.42, 0.74
Equivalent weight of MEM [10]	EW	0.95 $\mathrm{kg.mol^{-1}}$
Electrochemically active surface area [10]	$\mathrm{a_{ECSA}}$	70 $\mathrm{m^2_{Pt}/g_{Pt}}$
Absolute permeabilities of GDL, CL [15]	$\mathrm{K_{GDL}}, \mathrm{K_{CL}}$	1e-13, 2e-17 $\mathrm{m^2}$
Thermal conductivities of GDL, MEM [16]	$\sigma_{\mathrm{GDL}}, \sigma_{\mathrm{mem}}$	3, 0.37 $\mathrm{W.m^{-1}.K^{-1}}$

2.2 Governing Equations

The current model is governed by the conservation of mass and momentum for reactant gases, gas species, liquid pressure, electronic and ionic potential, dissolved water, and energy equations. These governing equations together with the solution domains are described in the following section while the reader is referred to reference [14] for more details on source terms of conservation equations and parameters.

Mass (Eq. 1) and momentum (Eq. 2) of the gas mixture are solved in channels, GDLs, and CLs:

$$\nabla.\left(\rho_{\mathrm{g}}\overrightarrow{\mathrm{u_g}}\right) = S_m \tag{1}$$

$$\rho_{\mathrm{g}}\overrightarrow{\mathrm{u_g}}.\nabla\overrightarrow{\mathrm{u_g}} = -\nabla \mathrm{p_g} + \mu\nabla^2\overrightarrow{\mathrm{u_g}} - \frac{\mu}{\mathrm{k}}\overrightarrow{\mathrm{u_g}} \tag{2}$$

Since the inertial terms could be neglected for the flow distribution in GDLs, and CLs, the left-hand side of Eq. 2 is zero for these domains.

Gas species distribution is solved for channels, GDLs, and CLs:

$$\nabla.\left(\rho_g w_i \sum_j D_{ij}\nabla X_j\right) + \rho_g\left(\overrightarrow{u_g}.\nabla\right)w_i = S_i \tag{3}$$

In Eq. 3, D_{ij} is binary diffusion coefficients of the species in channels and the sum of all the species mass fraction $(\sum w_i)$ is equals to 1. Thus, the gas species equation is applied for two out of three species.

Liquid pressure is solved for GDLs:

$$\nabla.\left(\frac{\rho_l\, k_l}{\mu_l}\nabla p_l\right) = S_l \tag{4}$$

Where, k_l is the effective permeability of GDL achieved from the multiplication of absolute permeability by the relative permeability based on the PSD mathematical model.

Electronic and ionic potentials are solved for GDLs, CLs, and the membrane:

$$\nabla.(-\sigma_s\nabla\phi_s) = S_{\phi s} \tag{5}$$

$$\nabla.(-\sigma_m\nabla\phi_m) = S_{\phi m} \tag{6}$$

The membrane is treated as a thin layer resisting the transport of ions as well as conducting the protons and dissolved water by adsorption and desorption processes through the anode and cathode sides.

$$\nabla.\left(\frac{\rho_{mem}}{EW}D_{H2O}^{Naf}\nabla\lambda\right) + \nabla.\left(\frac{n_d}{F}\sigma_l\nabla\phi_l\right) = S_\lambda \tag{7}$$

The energy equation is solved for the entire domain,

$$(\rho C_p)_{eff}\vec{u}.\nabla T + \nabla.\left(-k_{eff}\nabla T\right) = S_T \tag{8}$$

The description and units of the above-mentioned parameters are described in reference [14].

2.3 Catalyst Sub Model

To account for the structure of the cathode catalyst layer, the kinetic rate equation in reference [5] is adopted. The available oxygen in the pores of CL dissolves into the ionomer, then diffuses through the ionomer film, and lastly adsorbs on the surface of Pt particles participating in the electrochemical reaction. Thus, the total local transport resistance is,

$$R_T = R_{w,int} + \frac{\delta_w}{D_{O2,w}} + R_{e,int} + \frac{\delta_e}{D_{O2,ion}} + R_{Pt,int} \tag{9}$$

In which the second and fourth fractional terms describe the diffusional resistance, and the other terms

represent the interfacial resistances. Interfacial resistances are assumed to be proportional to diffusional resistances using fitting parameters,

$$R_{w,int} = k_3 \frac{\delta_w}{D_{O_2,w}}, R_{e,int} = k_1 \frac{\delta_e}{D_{O2,ion}}, R_{Pt,int} = k_2 \frac{\delta_e}{D_{O2,ion}} \quad (10)$$

The concentration of oxygen on the surface of Pt particles $(C_{O_2}^{Pt})$ can be calculated as follows,

$$i_{ORR}(C_{O_2}^{Pt})^{\gamma} + \frac{4F}{R_T/(a_c x)}(C_{O_2}^{Pt} - C_{O_2}^{g}) = 0 \quad (11)$$

In Eq. 11, $i_{0c}, \alpha_{ca}, \eta_{ca}, \gamma, w$ are the cathode exchange current density, transfer coefficient, cathodic overpotential, reaction order, and Temkin energy parameter respectively.

A modified Tafel expression is considered to account for the surface coverage to obtain the reaction ORR kinetics [17],

$$i_{ORR} = i_{0,c} a_{Pt}(1 - \theta_{PtO})(\frac{C_{O_2}^{Pt}}{C_{O_2}^{ref}})^{\gamma} \exp\left(\frac{-F\alpha_{ca}\eta_{ca}}{RT} - \frac{w\theta_{PtO}}{RT}\right) \quad (12)$$

where a_c, x are the volumetric surface area of ionomer film covering the carbon particles, and the total number fraction of Pt/C particles,

$$x = \frac{(1 - wt\%)(1 - y_{bare})}{1 - wt\%(1 - y_{bare})} \quad (13)$$

In Eq. 13, y_{bare} is the mass fraction of bare carbon particles. A simplified sigmoidal function is utilized for oxide coverage over Pt particles considering its dependence on the potential [17],

$$\theta_{PtO} = \left[(1 + e^{22.4(0.818 - V_{cell})})\right]^{-1} \quad (14)$$

In which V_{cell} is the cathode potential vs. reference hydrogen electrode (RHE),

$$V_{cell} = V_{rev} - \eta_{ca} - \eta_{an} - \Delta V_m - \Delta V_{CL} - \Delta V_{ohm} \quad (15)$$

where $V_{rev}, \Delta V_m, \Delta V_{ohm}$ are the reversible cell potential, the resistance of the electrolyte phase, and ohmic resistance of the components respectively [14] while η_{ca} is the overpotential in cathode calculated from Eq. 11, and η_{an} is anode electrode overpotential obtained from,

$$i_{OHR} = i_{0,a} a_{Pt}(\frac{C_{H_2}^{Pt}}{C_{H_2}^{ref}})^{\gamma} \exp\left(\frac{F\alpha_{an}\eta_{an}}{RT}\right) \quad (16)$$

Considering the ionomer content in CL, ΔV_{CL} is added to the model to account for proton conductivity based on the experimental data measured by reference [18],

$$\Delta V_{CL} = R_{ion,CL} J_{cell} \delta_{CL}(1 - y_{bare})^{-0.25} \quad (17)$$

While the $R_{ion,CL}$ can be calculated from [18],

$$R_{ion,CL} = \tau/\kappa_{(T,RH)}\varepsilon_{CL} \quad (18)$$

where the τ is tortuosity, which in the most general case is dependent on porosity, and κ is the proton conductivity of ionomer fitted from experiments [18]. Lastly, a_{Pt} is the active volumetric surface area of Pt dependent on the Pt loading and electrochemical specific area (a_{ECSA}),

$$a_{Pt} = a_{ECSA} L_{Pt}/\delta_{CL} \quad (19)$$

The reader is referred to reference [5] for more information and details regarding the catalyst layer model.

2.4 Mixed Wettability PSD

In this work, the mixed wettability model with individual PSDs for HI and HO pores and discrete values of contact angles is utilized. The water retention curves, relative permeabilities, Knudsen radii, and liquid-gas interfacial area are obtained from the volume fractions and characteristics radii, and contact angles of HI and HO pores. Since the Knudsen diffusion effect is dominant in relatively small pores, the Knudsen radius is only considered for CL. Furthermore, the microstructural properties of a Mitsubishi Rayon Co. (MRC) 105 are adopted for GDL [15] while the properties of graphitized Ketjen Black carbon support (GKB) are used to obtain the essential parameters of CL [19].

2.5 Model Validation

All the simulations of the current study are performed using COMSOL Multiphysics software. The numerical model developed is first applied for novel electrode compositions provided by reference [10] for which all the structural CL parameters are reported in Table 2. In their experiments, different *wt%* of Pt particles are diluted with bare carbon particles maintaining the thickness of CL [10]. Thus, the distribution of catalyst influential particles including the Pt and carbon particles is different, which affect the transport resistances and polarization curves. The comparison of simulated and experimental data [10] for both diluted and non-diluted catalysts is represented in Fig. 2.

The predicted polarization curves for air feed shows good agreement with experiments for both dilution and non-dilution cases. Owing to the reduced oxygen concentration in cathode CL, the performance of low Pt-loaded catalysts has deteriorated. This concentration drop is mostly related to the significant transport resistances occurring near the reaction sites. For the diluted catalysts, the number fraction of Pt/C particles available for the electrochemical reaction is decreased while the concentration of oxygen adjacent to active sites is increased greatly.

3. RESULTS AND DISCUSSION

3.1 Effect of Bare Carbon Mass Fraction

Since the thickness of the CL is kept constant in Fig. 2 for various fractions of bare carbon, the macroscopic catalytic structure is identical while the various *wt%* of Pt is utilized, and additional carbon is supplied upon necessity [10]. Assuming uniform coverage of ionomer film on the surface of carbon particles, a consistent flux is provided for non-dilution catalysts while the flux of oxygen is concentrated on the rare Pt/C particles in diluted catalysts. Comparing the results for different Pt loadings, the considerable performance drop is discernable for diluted catalysts, especially for Pt loading of 0.025 $(\mathrm{mg_{Pt}/cm^2})$ which is directly related to the intensified transport resistances.

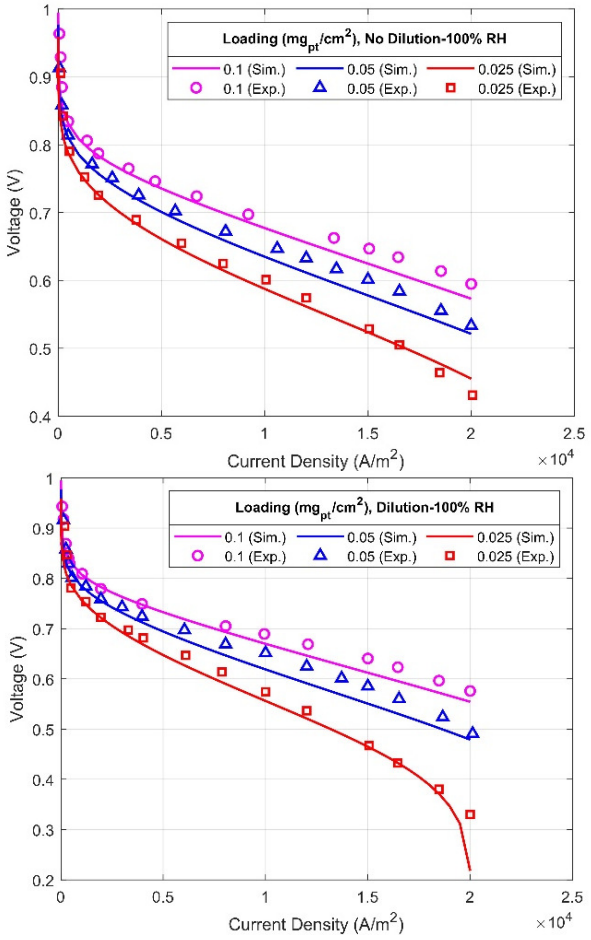

Fig. 2. Model validation with experimental data [10] for 100% RH, 80°C, and 1.5 atm operating conditions for non-diluted (up) and diluted catalysts (down)

Table 2

CL design parameters [10]

Pt loading (mg_{Pt}/cm^2)	*Carbon Dilution*	y_{bare}	*wt%*
0.1	✓	*0.58*	*0.5*
0.05	✓	*0.78*	*0.5*
0.025	✓	*0.89*	*0.5*
0.1	✗	-	*0.3/0.15*
0.05	✗	-	*0.1*
0.025	✗	-	*0.05*

3.2 Effect of Ionomer to Carbon Ratio

The I/C ratio is one of the deterministic parameters during the manufacturing process. Increasing the ionomer content results in enhanced transfer of protons and higher content of water in the ionomer. However, the oxygen diffusion and active reaction surface area both are decreased due to the occupation of CL pores by the ionomer. To study the effect of I/C, three different values, 1.5, 0.95 and 0.5, are numerically simulated and the polarization curves are compared in Fig. 3. Pt loading of 0.1 (mg_{Pt}/cm^2) and a non-diluted catalyst is used for obtaining results in the following sections.

The performance depends strongly on the I/C ratios. In this study, the proton conductivity of CL is obtained from the experimental data provided by reference [18], and reducing the ionomer content in CL causes lower proton conductance which significantly decreases the performance for the I/C ratio of 0.5.

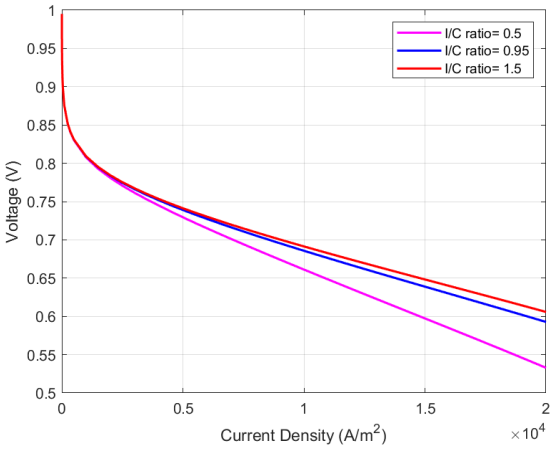

Fig. 3. Effect of I/C ratios on performance

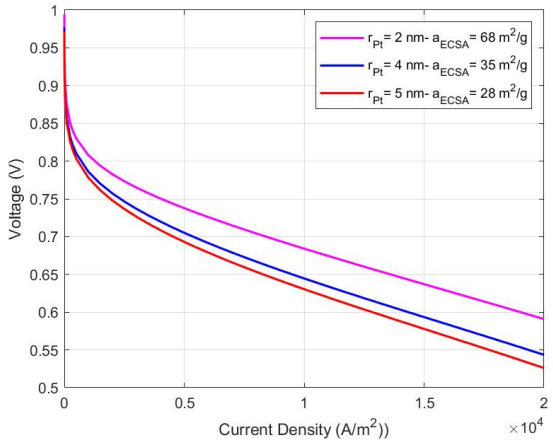

Fig. 4. Effect of Pt particles radius on performance

3.3 *Effect of CL Particles*

The effect of Pt particle radius is studied using three different values of 2, 4, and 5 nm. At the nanoscale, the ratio of surface area to volume decreases with increasing

particle radius. Thus, using larger Pt particles reduces the active electrochemical surface area available for ORR reaction and results in lower performance as shown in Fig. 4.

Moreover, the simulated polarization curves for three carbon support radii of 10, 60, and 100 nm are shown in Fig. 5. A larger carbon support radius intensifies the transport resistance related to the diffusion of oxygen through the ionomer and its dissolution at the ionomer surface heightening the oxygen flux adjacent to reaction sites.

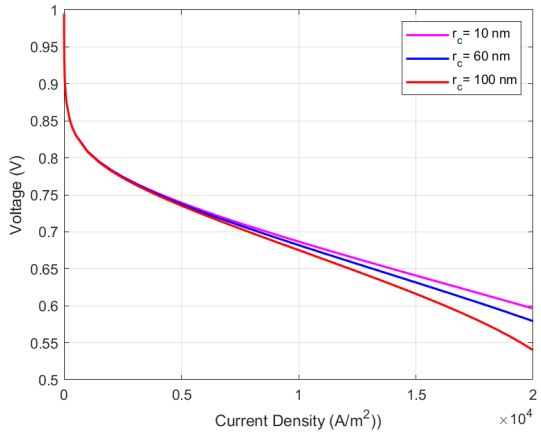

Fig. 5. Effect of carbon support radius on performance

4. CONCLUSION

A homogeneous catalyst layer accounting for the interfacial resistances through the oxygen path is incorporated into the 2D non-isothermal multi-phase PEMFC model here. The microstructural parameters are also included for the porous layers to obtain two-phase flow within the computational domain. The model is highly efficient for studying various cathode compositions and Pt loadings owing to the good agreement of predicated polarization curves with experimental data reported by Owejan *et al.* [10] as well as its low computational cost. The numerical model is further utilized to investigate four different CL design parameters. The diluted catalysts represent lower performance due to the increased flux adjacent to Pt particles. Furthermore, higher ionomer content in CL facilitates the proton conductance and eventually enhances the performance. Moreover, the radius of carbon support negatively affects the performance owing to the increased transport resistances, especially at high current densities. Lastly, Pt particles radius is an essential CL parameter since the electrochemically active surface area is directly dependent on its value. Therefore, decreasing the radius of Pt particles elevates the performance but it is bounded by the manufacturing limitations. This model will be extended to study the effects of operating conditions.

ACKNOWLEDGEMENT

This work was supported by The Scientific and Technological Research Council of Turkey, TUBITAK-119M388.

REFERENCES

[1] Sui PC, Zhu X, Djilali N. Modeling of PEM Fuel Cell Catalyst Layers: Status and Outlook. vol. 2. Springer Singapore; 2019.

[2] Huang J, Li Z, Zhang J. Review of characterization and modeling of polymer electrolyte fuel cell catalyst layer: The blessing and curse of ionomer. Frontiers in Energy 2017;11:334–64.

[3] Greszler TA, Caulk D, Sinha P. The Impact of Platinum Loading on Oxygen Transport Resistance. Journal of The Electrochemical Society 2012;159:F831–40.

[4] Siegel NP, Ellis MW, Nelson DJ, von Spakovsky MR. Single domain PEMFC model based on agglomerate catalyst geometry. Journal of Power Sources 2003;115:81–9.

[5] Hao L, Moriyama K, Gu W, Wang C-Y. Modeling and Experimental Validation of Pt Loading and Electrode Composition Effects in PEM Fuel Cells. Journal of The Electrochemical Society 2015;162:F854–67.

[6] Iden H, Sato K, Ohma A, Shinohara K. Relationship among Microstructure, Ionomer Property and Proton Transport in Pseudo Catalyst Layers. Journal of The Electrochemical Society 2011;158:B987.

[7] Ohma A, Mashio T, Sato K, Iden H, Ono Y, Sakai K, et al. Analysis of proton exchange membrane fuel cell catalyst layers for reduction of platinum loading at Nissan. Electrochimica Acta 2011;56:10832–41.

[8] Suzuki T, Kudo K, Morimoto Y. Model for investigation of oxygen transport limitation in a polymer electrolyte fuel cell. Journal of Power Sources 2013;222:379–89.

[9] Muzaffar T, Kadyk T, Eikerling M. Tipping water balance and the Pt loading effect in polymer electrolyte fuel cells: a model-based analysis. Sustainable Energy & Fuels 2018;2:1189–96.

[10] Owejan JP, Owejan JE, Gu W. Impact of Platinum Loading and Catalyst Layer Structure on PEMFC Performance. Journal of The Electrochemical Society 2013;160:F824–33.

[11] Zhou J, Putz A, Secanell M. A Mixed Wettability Pore Size Distribution Based Mathematical Model for Analyzing Two-Phase Flow in Porous Electrodes. Journal of The Electrochemical Society 2017;164:F530–9.

[12] Weber AZ, Darling RM, Newman J. Modeling Two-Phase Behavior in PEFCs. Journal of The Electrochemical Society 2004;151:A1715.

[13] Abdiel P, Villanueva M. A MIXED WETTABILITY PORE SIZE DISTRIBUTION MODEL FOR THE ANALYSIS OF WATER TRANSPORT IN PEMFC MATERIALS. n.d.

[14] Rizvandi OB, Yesilyurt S. A pseudo three-dimensional, two-phase, non-isothermal model of proton exchange membrane fuel cell. Electrochimica Acta 2019;302:180–97.

[15] Zenyuk I v., Parkinson DY, Connolly LG, Weber AZ. Gas-diffusion-layer structural properties under compression via X-ray tomography. Journal of Power Sources 2016;328:364–76.

[16] Kim S, Mench MM. Investigation of Temperature-Driven Water Transport in Polymer Electrolyte Fuel Cell: Phase-Change-Induced Flow. Journal of The Electrochemical Society 2009;156:B353.

[17] Subramanian NP, Greszler TA, Zhang J, Gu W, Makharia R. Pt-Oxide Coverage-Dependent Oxygen Reduction Reaction (ORR) Kinetics. Journal of The Electrochemical Society 2012;159:B531–40.

[18] Liu Y, Murphy MW, Baker DR, Gu W, Ji C, Jorne J, et al. Proton Conduction and Oxygen Reduction Kinetics in PEM Fuel Cell Cathodes: Effects of Ionomer-to-Carbon Ratio and Relative Humidity. Journal of The Electrochemical Society 2009;156:B970.

[19] Mashio T, Sato K, Ohma A. Analysis of Water Adsorption and Condensation in Catalyst Layers for Polymer Electrolyte Fuel Cells. Electrochimica Acta 2014;140:238–49.